Pressure-driven membrane inflation through nanopores on the cell wall

Qi Zhong[1], Chen-Xu Wu [1,2] Rui Ma[1,2,*],

1 Department of Physics, College of Physical Science and Technology, Xiamen University, Xiamen 361005, China
2 Fujian Provincial Key Lab for Soft Functional Materials Research, Research Institute for Biomimetics and Soft Matter, Xiamen University, Xiamen 361005, China

*** ruima@xmu.edu.cn**

Abstract

Walled cells, such as plants and fungi, compose an important part of the model systems in biology. The cell wall primarily functions to prevent the cell from over-expansion when exposed to water, and is a porous material distributed with nanosized pores on it. In this paper, we study the deformation of a membrane patch by an osmotic pressure through a nanopore on the cell wall. We find that there exists a critical pore size beyond which the membrane cannot stand against the pressure and would inflate out through the pore. The critical pore size scales exponentially with the membrane tension and the spontaneous curvature, and exhibits a power law dependence on the osmotic pressure. Our results also show that the liquid membrane expansion by pressure is mechanically different from the solid balloon expansion, and predict that the bending rigidity of the membrane in walled cells should be larger than that of the mammalian cells so as to prevent inflation through the pores on the cell wall.

Introduction

The cell wall is a structure that surrounds the cells of many organisms, including plants, fungi, bacteria, and some protists [1–4]. It is a rigid layer that provides support, protection, and shape to the cell. In plants, the cell wall is composed primarily of cellulose, a polysaccharide made up of glucose units [5]. The cell wall of fungi is composed of chitin, a polymer of N-acetylglucosamine [6, 7]. Bacterial cell walls are made up of peptidoglycan, a polymer of amino sugars and amino acids [8, 9]. The cell wall plays an important role in maintaining the integrity of the cell and protecting it from mechanical stress, osmotic pressure, and other environmental factors.

Basically, the cell wall is a porous structure that allows for the exchange of materials between the cell and its environment. The size and shape of the pores in the cell wall can vary depending on the type of cell and the function of the wall. For example, in the primary cell wall of plant cells, the size of the pores can range from 10-20 nanometers to several micrometers in diameter, with the largest pores often found at the corners where adjacent cells meet [10, 11]. In fungal cell walls, the size of the pores can also vary, but is typically at an order of a few tens of nanometers [12, 13].

Walled cells generally have a high osmotic pressure that allows them to grow and survive in the environment [14–19]. The osmotic pressure pushes the plasma membrane

against the cell wall and therefore prevents some important biological process from happening. In particular, endocytosis which involves the internalization of a small patch of plasma membrane is hindered by the osmotic pressure [20]. In fission yeast, the turgor pressure is estimated to be 0.85 ± 0.15 MPa by measuring the growth curve of a mutant yeast cell against a PDMS chamber [21, 22]. In another experiment which compares the geometry of a fission yeast cell upon osmolarity change, it is estimated that the turgor pressure is up to 1.5 ± 0.2 MPa [14]. Based on a similar osmolarity variation method, the value of turgor pressure is estimated to be 0.6 ± 0.2 MPa in budding yeast [23]. In general, the turgor pressure in yeast cells have an order of magnitude $0.1 - 1$ MPa.

In this work, we study membrane deformation through a nanopore on the cell wall by the osmotic pressure with the Helfrich model. We find that when the pore is small, the membrane assumes a certain shape to resist the osmotic pressure. When gradually increasing the pore size beyond a critical value, the membrane cannot stand against the pressure anymore and would inflate out through the pore and further expand. We systematically study how the critical pore size R_{crit} depends on the membrane properties and find that R_{crit} scales exponentially with the membrane tension and the spontaneous curvature, but scales with the osmotic pressure with a power law. We show that the expansion of a liquid membrane by pressure is different from a solid one in terms of their p-V curve. Our results suggest that the membrane bending rigidity in walled cells should be larger than that in mammalian cells so as to prevent the cell from inflation through the nanopores present on the cell wall.

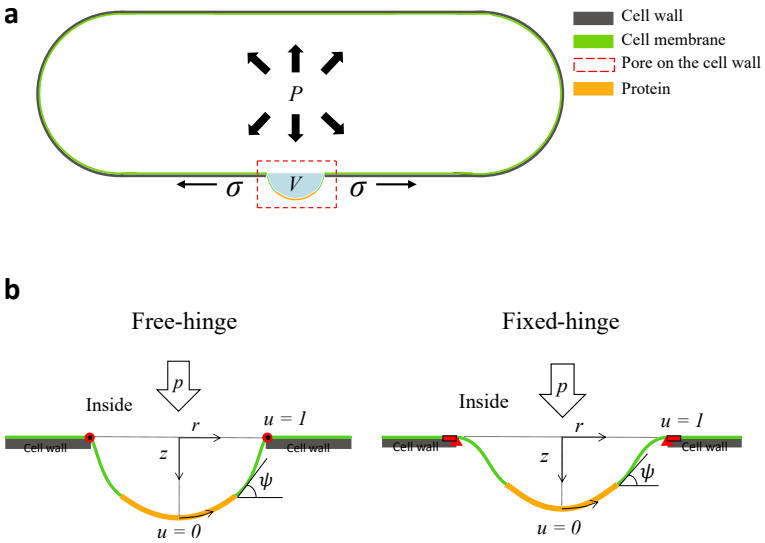

Figure 1. Schematic illustration of a typical yeast cell and the model. (a) Illustration of the typical morphology of a fission yeast cell. A nanopore (red frame) is present on the cell wall (gray) and the membrane (green) is pushed outwards by the osmotic pressure p. The size of the nanopore is exaggerated for the purpose of illustration only. **(b)** Illustration of the membrane models. The membrane shape is assumed to be axisymmetric with respect to the z-axis, and parameterized by its meridinal coordinates $[r(u), z(u)]$ with $u = 0$ labeling the membrane tip and $u = 1$ labeling the membrane edge. Two types of boundary conditions (BCs) are considered, namely the free-hinge BC (left) in which the membrane is allowed to freely rotate at the pore edge and the fixed-hinge BC (right) in which the membrane angle is fixed. The proteins (orange) coated on the membrane are assumed to generate the spontaneous curvature of the membrane.

Methods

Model

We consider a walled cell with a high osmotic pressure p that pushes the cell membrane against the cell wall. A nanopore with a radius of R_{pore} is present on the cell wall, which has a much larger Young's modulus than the osmotic pressure and a much smaller curvature than the nanopore [24–27]. The cell wall is therefore modeled as a rigid and flat substrate. We assume the deformation of the membrane at the pore is axisymmetric, and parameterized with its meridional coordinates $[r(u), z(u)]$, where $u \in [0, 1]$ is the rescaled arclength. The point at $u = 0$ labels the membrane tip and the points at $u = 1$ label the membrane edge (Fig. 1b). The coordinates satisfy the geometric relations

$$r' = h\cos\psi, \qquad z' = -h\sin\psi. \tag{1}$$

Hereafter, we use f' to denote the derivative of an arbitrary function f with respect to u. The angle $\psi(u)$ spans between the tangential direction and the horizontal direction. The constant h is essentially the total arclength of the membrane profile and is to be solved with the shape equations. The total energy of the membrane reads

$$G = \frac{\kappa}{2}\int (c_1 + c_2 - c_0)^2 dA + \sigma A + pV, \tag{2}$$

where the first term is the classical Helfrich bending energy with κ denoting the bending rigidity of the membrane, $c_1 = \dot{\psi}/h$ and $c_2 = \sin\psi/r$ the two principal curvatures of the membrane surface, c_0 denoting the spontaneous curvature induced by curvature-generating proteins coated on the membrane [28, 29]. In the absence of proteins, the spontaneous curvature is assumed to vanish. The second term in Eq. (2) is the surface tension energy with A denoting the surface area of the deformed membrane, and σ denoting the membrane tension at the edge of the pore. The third term describes the effect of the osmotic pressure with V being the increased volume of the membrane due to inflation, and p denoting the osmotic pressure (Fig. 1a). Due to the rotational symmetry of the membrane shape about the z axis, the total energy of the membrane in Eq. (2) can be expressed as a functional of the shape variables

$$G = 2\pi\int_0^1 L[\psi, \psi', r, r', z, z', h, \gamma, \eta]du. \tag{3}$$

Here γ, η are Lagrangian multipliers that enforce the geometric relations in Eq. (1). The shape equations of the membrane are obtained by applying variations of the free energy G with respect to all the shape variables [30, 31]. The variation δG contains both bulk terms, e.g., $[\partial L/\partial\psi - d(\partial L/\partial\psi')/du]\,\delta\psi$, and boundary terms, e.g., $(\partial L/\partial\psi')\delta\psi|_{u=0}^{u=1}$. We obtain the shape equations by having the bulk terms to be zero. In addition, proper boundary conditions (BCs) at the membrane tip $u = 0$ and at the pore edge $u = 1$ need to be specified, which can be achieved by setting the boundary terms in δG to be zero. There are two types of BCs, the free-hinge BC in which the membrane angle ψ is allowed to freely rotate, and the fixed-hinge BC in which the membrane angle ψ is fixed to be 0 (Fig. 1b). They correspond to have either $\partial L/\partial\psi' = 0$ or $\delta\psi = 0$ in the boundary term. The detailed derivation of the shape equations and the BCs is provided in the appendix.

We numerically solve the shape equations with the bvp4c solver in MATLAB, which is designed for solving boundary value problems (BVPs) of ordinary differential equations.

Results

Critical pore size for membrane inflation scales exponentially with the membrane tension and spontaneous curvature.

In this section, we fix the osmotic pressure p and study how the membrane is deformed when gradually increasing the pore radius $R_{\rm pore}$. The osmotic pressure p and the membrane bending rigidity κ define a characteristic length $R_{\rm p} = (\kappa/2p)^{1/3}$, which is used to rescale the length, and nondimensionalize all the other parameters. In particular, the rescaled pressure $\bar{p} = pR_{\rm p}^3/\kappa = 0.5$ is a constant. The other nondimensionalized parameters include the rescaled tension $\bar{\sigma} = \sigma R_{\rm p}^2/\kappa$, and the rescaled spontaneous curvature $\bar{c}_0 = c_0 R_{\rm p}$.

We first consider a membrane without any curvature-generating proteins and study how the membrane is deformed when continuously increasing the radius of the pore $R_{\rm pore}$ under a constant membrane tension $\bar{\sigma} = 0.001$. The membrane is pushed down by the pressure p to a depth of $D_{\rm pore}$. It is found in the $D_{\rm pore} - R_{\rm pore}$ curve, a single value of the pore radius $R_{\rm pore}$ corresponds to two membrane shapes (squares and circles in Fig. 2 c), one with a shallow depth and the other with a deep one. By comparing the total energy of the two shapes (Fig. 2 b), we see that the energy of the shallow solution is much lower than that of the deep one, indicating an energetically more favorable state of the membrane. For the shallow shapes, the depth of the membrane is pushed further down by the pressure as the pore size is enlarged, while for the deep shapes, the depth of the membrane shows a nonmonotonic relation with the pore radius. There exists a critical pore size $R_{\rm crit}$ beyond which no solutions are found, which indicates that the osmotic pressure is too strong for any membrane shape to sustain the pressure. The membrane would continuously inflate out of the pore and expand over time if there is constant supply of lipid molecules flowing into the pore from the edge.

We then plot the $D_{\rm pore}$ vs. $R_{\rm pore}$ curves for different membrane tensions $\bar{\sigma}$ (Fig. 2)d. The critical pore size $\bar{R}_{\rm crit}$ is found to strongly depend on the membrane tension $\bar{\sigma}$. For $\bar{\sigma} < 0.1$, the critical radius $\bar{R}_{\rm crit}$ stays around 2. Beyond $\bar{\sigma} = 0.1$, $\bar{R}_{\rm crit}$ has a dramatic increase with $\bar{\sigma}$ (Fig. 2e, green dotted curve). The relationship can be nicely fitted with an exponential function (Fig. 2 e, cyan dashed curve).

We next consider a membrane totally coated by proteins and study the effect of spontaneous curvature c_0 induced by the proteins on the membrane deformation, particularly on the critical pore radius. The $D_{\rm pore} - R_{\rm pore}$ curve for a coated membrane with positive $\bar{c}_0$ show a similar trend with that of the uncoated membrane, i.e., a single pore radius corresponding to two solutions, one with a lower energy and the other with a higher one (Fig. 3a, b). However, solutions with negative depth appear for small pore radii in the lower energy branch due to the positive spontaneous curvature c_0 that tends to bend the membrane inward against the osmotic pressure (Fig. 3a). When the pore radius becomes large, the spontaneous curvature c_0 cannot resist the osmotic pressure anymore and the membrane is pushed outward by the pressure (Fig. 3c). The $D_{\rm pore} - R_{\rm pore}$ curves for different spontaneous curvatures c_0 are shown in Fig. 3d. The critical radius increases with the spontaneous curvature and the relationship can be well fitted by an exponential function (Fig. 3e).

Critical pressure for membrane inflation scales with the pore radius with a power law

In this section, we fix the pore radius and study how an uncoated membrane is deformed by gradually increasing the osmotic pressure p. The membrane tension σ and the membrane bending rigidity κ defines a characteristic length $R_\sigma = [\kappa/(2\sigma)]^{1/2}$, which is

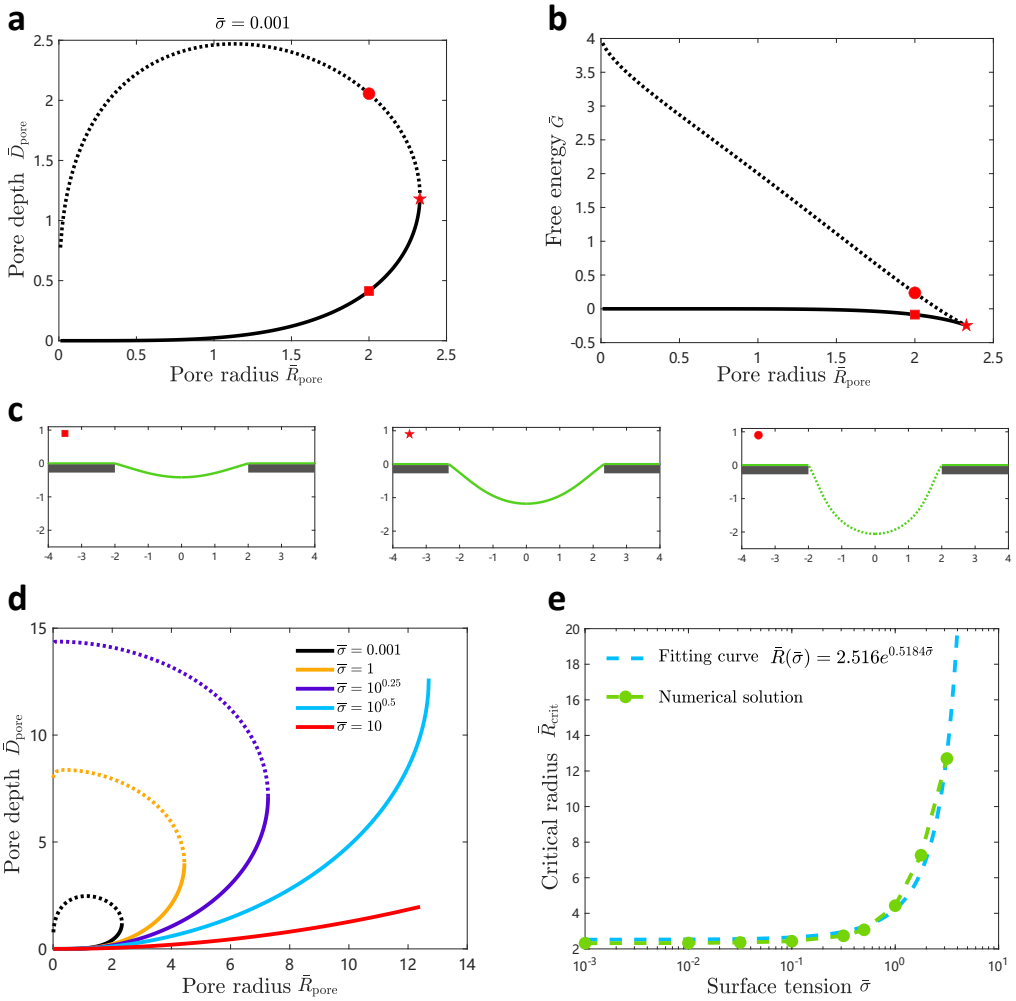

Figure 2. Effect of the surface tension on the critical radius of an uncoated membrane. **(a)** $D_{\rm pore}$ vs. $R_{\rm pore}$ curve of membrane deformations for an uncoated membrane. The critical pore size, beyond which no solutions are found, is indicated by a pentagon. **(b)** The free energy curve of the corresponding membrane deformations in (a). The solid curve indicates a stable state, and the dashed line indicates a metastable state. **(c)** Illustration of the membrane shapes indicated by the corresponding symbols on the $D_{\rm pore}$ vs. $R_{\rm pore}$ curve. **(d)** $D_{\rm pore}$ vs. $R_{\rm pore}$ curves are shown for different membrane tensions $\bar{\sigma}$. **(e)** The critical pore size as a function of the surface tension $\bar{\sigma}$. The green dotted curve represents the numerical solutions. The cyan dashed curve represents the exponential fitting of the numerical solution.

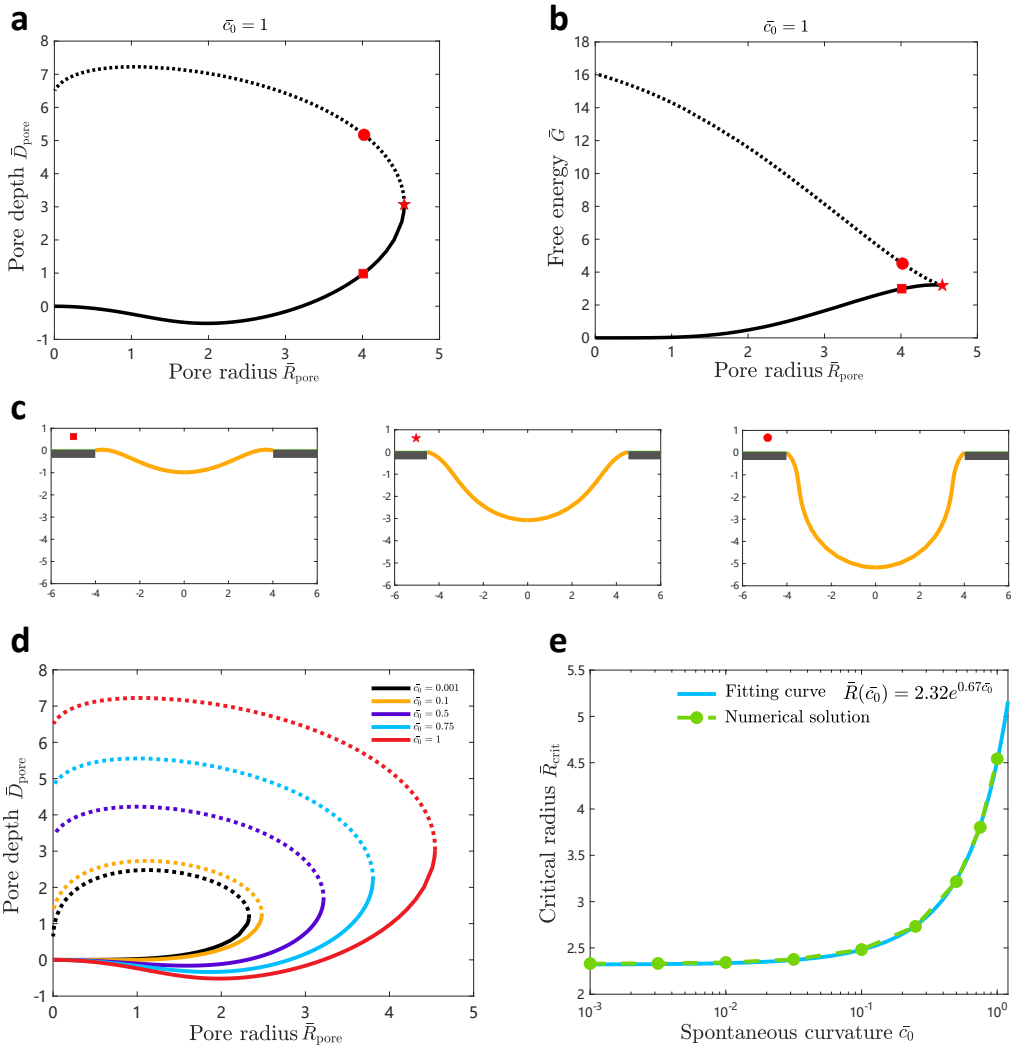

Figure 3. Effect of the spontaneous curvature on the critical radius of a totally coated membrane. **(a)** $D_{\rm pore}$ vs. $R_{\rm pore}$ curve of membrane deformations for a totally coated membrane with spontaneous curvature $\bar{c}_0 = 1$. The critical pore size is indicated by a pentagon. **(b)** The free energy curve of the corresponding membrane deformations in (a). The solid line indicates a stable state, and the dashed line indicates a metastable state. **(c)** Illustration of the membrane shapes indicated by the corresponding symbols on the $D_{\rm pore}$ vs. $R_{\rm pore}$ curve. **(d)** $D_{\rm pore}$ vs. $R_{\rm pore}$ curves are shown for different spontaneous curvatures $\bar{c}_0$. **(e)** The critical pore size as a function of the spontaneous curvature $\bar{c}_0$. The green dotted curve represents the numerical solutions. The cyan dashed curve represents the exponential fitting of the numerical solution.

used to rescale the length, and nondimensionalize all the other parameters. In particular, the membrane tension can be rescaled to a constant $\bar{\sigma} = \sigma R_\sigma^2/\kappa = 0.5$. The rescaled osmotic pressure is $\bar{p} = pR_\sigma^3/\kappa$.

A typical $\bar{D}_{\rm pore}$ vs. $\bar{p}$ curve is shown in Fig. 4a. A single osmotic pressure $\bar{p}$ can find two corresponding depths on the curve (Fig. 4), with the shallow one having a lower energy and the deep one having a higher energy (Fig. 4b, c). We stress that for small osmotic pressure p, the high energy branch can have a very large depth. This is similar to the p-V curve of an inflating balloon [32–36]. When the osmotic pressure is a beyond a critical value, no solutions are found. It implies that the osmotic pressure is too large for any membrane shape to sustain the pressure. The membrane would inflate out of the pore to form a bulge. The critical pressure $\bar{p}_{\rm crit}$ is found to increase with the pore radius (Fig. 4d), and the relationship can be well fitted with a power law $\bar{p}_{\rm crit} = 6.978 R_{\rm pore}^{-2.899}$ (Fig. 4e).

Discussion

The critical pore size is about 10 nm given the typical parameters of the membrane

We have shown that if a nanopore is present on the cell wall and the pore radius is small, the membrane is able to resist the osmotic pressure by assuming a curved shape. If the pore radius is beyond a critical value $R_{\rm crit}$, no membrane shapes are able to sustain the osmotic pressure and the membrane would inflate out and further expand. In Fig. 5, we show how the critical pore size depends on the model parameters, given the typical value of the membrane properties. The model parameters include the bending rigidity κ, the membrane tension σ, the osmotic pressure p, and the spontaneous curvature c_0. We fix three of them to the typical values (listed on the top of each panel in Fig. 5), and vary the fourth one to see how it impacts the critical pore size R_{crit} using the fitted expression $\bar{R}_{\rm crit} = 2.516\exp(0.518\bar{\sigma})$ for the free-hinge BC and $\bar{R}_{\rm crit} = 3.468\exp(0.434\bar{\sigma})$ for the fixed-hinge BC. The critical pore size $R_{\rm crit}$ is found to decrease with the osmotic pressure and increase with the other three parameters, and stays in the range of $5 - 20$ nm. In general, $R_{\rm crit}$ is smaller under the free-higne BC than that under the fixed hinge BC. As we have pointed out, the typical pore size of the cell wall is about tens of nanometers [10–13], which is comparable to the critical pore size calculated by our theory (Fig. 5b). Our calculation therefore implies that the bending rigidity of the walled cells must be higher than the value 20 kT we have typically assumed. This is plausible based on the experimental evidence that the membrane is surrounded with actin meshwork in yeast cells [37–39], which is able to effectively increase the bending rigidity of the membrane. Furthermore, proteins on the membrane are also help to increase the bending rigidity.

Liquid membrane versus solid balloon

In Fig. 4, we have presented the results for the membrane deformation when gradually increasing the osmotic pressure. The $D_{\rm pore}$ vs. $\bar{p}$ curve is found to be nonmonotic, which resembles the p-V curve of an inflating balloon [32–36]. In practice, the setup shown in Fig. 4 is used to measure the elastic properties of solid polymer materials, such as rubber. However, for the solid balloon, in particular, at very large volume, the p-V curve would increase with the pressure again due to the stretching energy of the rubber that makes up the balloon. In our case, we consider an incompressible liquid membrane and the membrane area increase is due to the lipid flow from the pore edge when the membrane is pushed by the osmotic pressure. The membrane tension σ at the edge is fixed instead

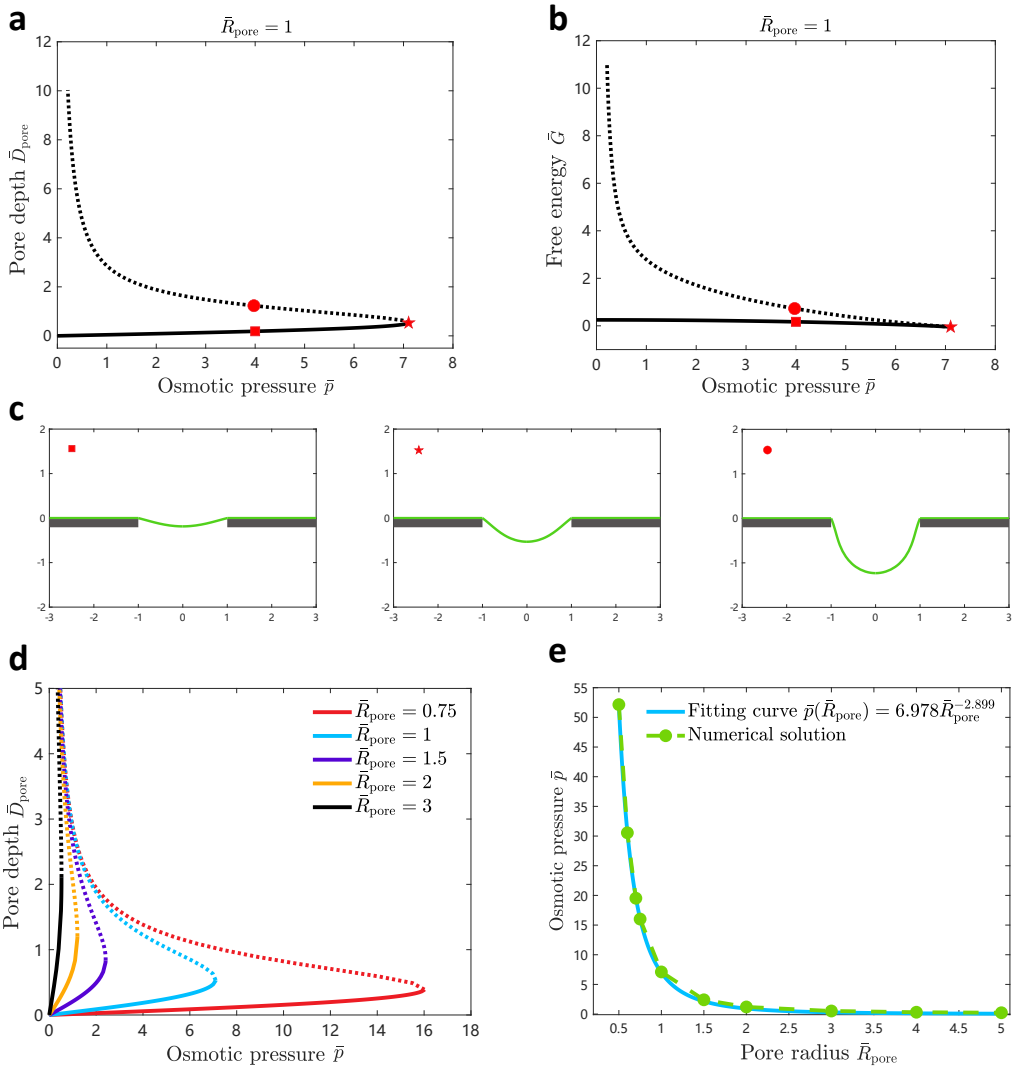

s

Figure 4. Effect of the osmotic pressure on the membrane deformation for an uncoated membrane. **(a)** D_{pore} vs. $\bar{p}$ curve of membrane deformations for an uncoated membrane. The pore size is fixed at $\bar{R}_{\text{pore}} = 1$. The critical osmotic pressure is indicated by a pentagon. **(b)** The free energy curve of the corresponding membrane deformations in (a). The solid curve indicates a stable state and the dashed curve indicates a metastable state. **(c)** Illustration of the membrane shapes indicated by the corresponding symbols on the D_{pore} vs. $\bar{p}$ curve. **(d)** D_{pore} vs. $\bar{p}$ curves are shown for different pore size $\bar{R}_{\text{pore}}$. **(e)** The critical pressure as a function of the pore size $\bar{R}_{\text{pore}}$. The green dotted curve represents the numerical solutions. The cyan dashed curve represents the power law fitting of the numerical solution.

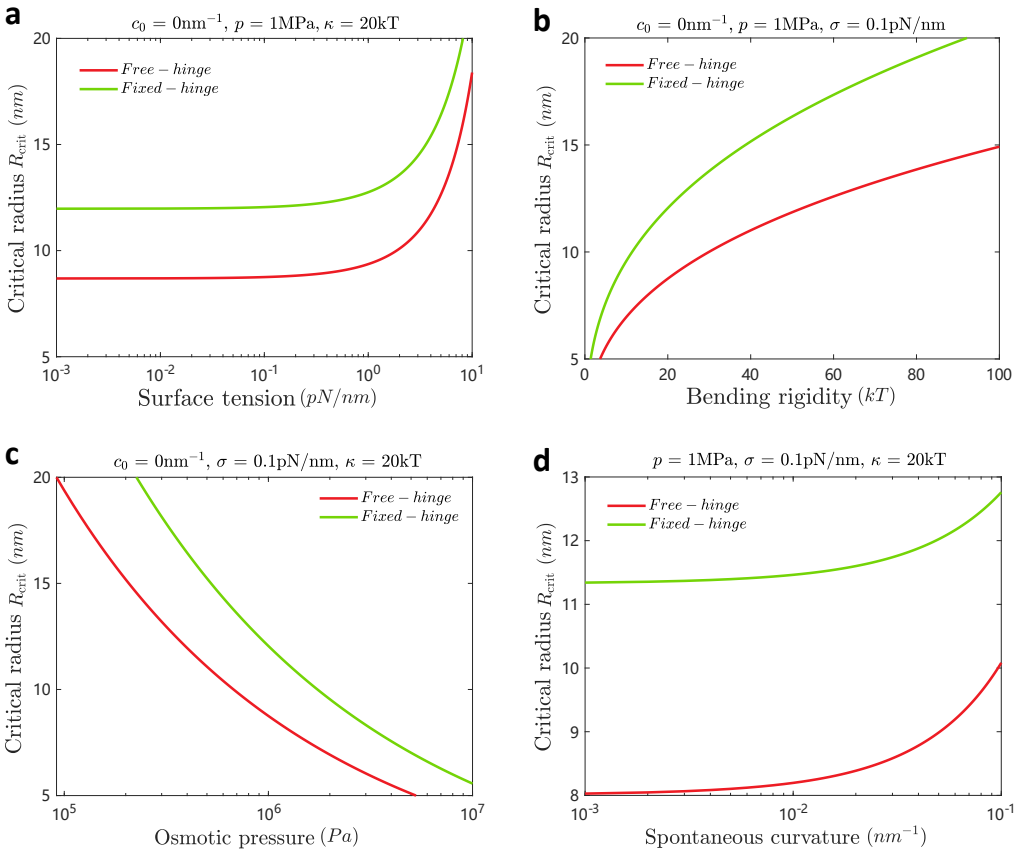

Figure 5. Dependence of the critical pore size on the model parameters. The typical values of the fixed parameters are listed on top of each panel. The red curve is for the free-hinge BC and the green curve is for the fixed-hinge BC. **(a-d)** The relationship between the critical radius R_{crit} and the surface tension σ, the bending rigidity κ, the osmotic pressure p, and the spontaneous curvature c_0, respectively.

of increasing with the depth. Therefore, we can find deep invaginations at very small pressure, which differs the liquid membrane from the solid balloon.

Conclusion

We have studied membrane inflation through a nanopore on the cell wall in the presence of a high osmotic pressure. It is found that there exists a critical value of the pore size $R_{\rm crit}$ beyond which the membrane cannot stand against the osmotic pressure and would inflate out through the pore and keep expansion. The critical pore size $R_{\rm crit}$ scales exponentially with the membrane tension σ and the spontaneous curvature c_0, and scales with the osmotic pressure p with a power law. The boundary conditions at the pore edge also make a quantitative difference. In general, the fixed-hinge BC leads to a larger $R_{\rm crit}$ than the free-hinge BC. Our results also reveal that the inflation of a liquid membrane by pressure behaves differently than that of a solid balloon. In walled cells where the osmotic pressure is high, the membrane should have a large bending rigidity than that in mammalian cells to prevent from inflation through the pores on the cell wall.

Appendix

Derivation of the membrane shape equations

In order to derive the membrane shape equations, we explicitly express the integrand L in Eq. (3) as

$$\begin{aligned} L = &\frac{1}{2}\kappa\left(\frac{\psi'}{h}+\frac{sin\psi}{r}-c_0\right)^2 rh + \frac{p}{2}r^2 h\sin\psi + \sigma hr \\ &+ \gamma(u)(r'-h\cos\psi) + \eta(u)(z'+h\sin\psi). \end{aligned} \tag{4}$$

Here the three terms in the first line describe the energy contribution made by the bending rigidity, the surface tension, and the osmotic pressure, respectively, and the two terms in the second line describe the Lagrangian multiplies $\gamma(u)$ and $\eta(u)$ to enforce the geometric constraints Eq. (1). The variation of the functional G in Eq. (3) reads

$$\begin{aligned} \frac{\delta G}{2\pi} = &\int_0^1 du\left[\left(\frac{\partial L}{\partial\psi}-\frac{d}{du}\frac{\partial L}{\partial\psi'}\right)\delta\psi + \left(\frac{\partial L}{\partial r}-\frac{d}{du}\frac{\partial L}{\partial r'}\right)\delta r + \left(\frac{\partial L}{\partial z}-\frac{d}{du}\frac{\partial L}{\partial z'}\right)\delta z\right] \\ &+ \int_0^1 du\left[\frac{\partial L}{\partial\gamma}\delta\gamma + \frac{\partial L}{\partial\eta}\delta\eta + \frac{\partial L}{\partial h}\delta h\right] \\ &+ \frac{\partial L}{\partial\psi'}\delta\psi\Big|_{u=0}^{u=1} + \frac{\partial L}{\partial r'}\delta r\Big|_{u=0}^{u=1} + \frac{\partial L}{\partial z'}\delta z\Big|_{u=0}^{u=1}. \end{aligned} \tag{5}$$

The variation contains both the bulk terms (first and second lines) and the boundary terms (third line). By letting the bulk terms equal to zero, we obtain a set of ordinary differential equations, which include a second-order equation

$$\psi'' = \frac{h^2\cos\psi\sin\psi}{r^2} - \frac{\psi'}{r}h\cos\psi + \frac{p}{2\kappa}rh\cos\psi + \frac{\gamma}{\kappa r}h^2\sin\psi + \frac{\eta}{\kappa r}h^2\cos\psi, \tag{6}$$

and two first-order equations

$$\gamma' = h\left[\frac{1}{2}\kappa\left(\frac{\psi'}{h}-c_0\right)^2 - \frac{\kappa\sin^2\psi}{2r^2} + \sigma + pr\sin\psi\right], \tag{7}$$

and

$$\eta' = 0, \tag{8}$$

as well as the two geometric relations in Eq. (1).

In addition, the equation $\partial L/\partial h = 0$ does not give an equation of h, but leads to a conserved quantity [30, 31]

$$\mathcal{H} \equiv \frac{\partial L}{\partial h} = \frac{\kappa}{2} r \left[\left(\frac{\psi'}{h} \right)^2 - \left(\frac{\sin\psi}{r} - c_0 \right)^2 \right] - \frac{p}{2} r^2 \sin\psi - \sigma r + \gamma \cos\psi - \eta \sin\psi = 0. \tag{9}$$

There is a freedom to choose the scale function h. Here we choose $h' = 0$ such that h is a constant to be determined. It is essentially the total arclength of the membrane profile.

Derivation of the boundary conditions

By letting the boundary terms in Eq. (5) equal to zero, we obtain the BCs. In particular, in the boundary term about δr, we let $\delta r\big|_{u=0}^{u=1} = 0$, which implies to fix the radius

$$r(0) = 0, \qquad r(1) = R_{\text{pore}}. \tag{10}$$

In the boundary term about δz, we obtain

$$\frac{\partial L}{\partial z'}(u = 0) = \eta(0) = 0, \qquad z(0) = 0. \tag{11}$$

As for the boundary term about $\delta\psi$, at the membrane tip, we have

$$\psi(0) = 0. \tag{12}$$

At the pore edge, we have two choices. If we let $\delta\psi(1) = 0$, it is equivalent to the fixed-hinge BC

$$\psi(1) = 0. \tag{13}$$

If we let $\partial L/\partial\psi' = 0$, it is equivalent to the free-hinge BC

$$\frac{\partial L}{\partial \psi'} = \kappa \left(\frac{\psi'}{h} + \frac{\sin\psi}{r} - c_0 \right) = 0. \tag{14}$$

The conserved quantity $\mathcal{H} = 0$ at the membrane tip $u = 0$ gives rise to a BC

$$\gamma(0) = 0. \tag{15}$$

Numerical methods to calculate the D_{pore} vs. R_{pore} curve

So far we have obtained a total number of 5 equations, which include Eqs. (1), (6), (8), (8). Since only Eq. (6) is first order, they are equivalent to a total number of 6 first order ordinary differential equations. In addition, Eqs. (10), (11), (12), (13) or (14) constitute a total number of 7 BCs. Overall, the 6 equations plus 1 unknown parameter h, and the 7 BCs constitute a well-defined boundary value problem.

We solve the problem with the matlab solver bvp5c, which requires the equations and the BCs as its input. Furthermore, the solver requires an initial guess of the solutions. In order to obtain the D_{pore} vs. R_{pore} curve, We always start with a small R_{pore} and use the flat shape as our initial guess. In this case, the membrane is almost flat, and it is easy for the solver to find the solution. We then gradually increase the pore radius R_{pore} to $R_{\text{pore}} + \Delta R$ and use the solution for R_{pore} as the initial guess to solve the equation

for $R_{\text{pore}} + \Delta R$. This iteration step allows us to extend the solution to the critical pore radius since beyond which no solutions are found anymore. We then use the solution at the critical pore radius as the starting point and iterate over the membrane depth D_{pore} to obtain the other branch of the solution. During this iteration, we add the boundary condition $z(0) = D_{\text{pore}}$ and set the pore radius R_{pore} as an unknown parameter to be solved by the solver.

Acknowledgments

We acknowledge financial support from National Natural Science Foundation of China under Grants No. 12004317, Fundamental Research Funds for Central Universities of China under Grant No. 20720200072, and 111 project No. B16029.

References

1. MCCANN, MC, WELLS, B, ROBERTS, and K. Direct visualization of cross-links in the primary plant-cell wall. *J Cell Sci*, 1990.

2. Pengjian Gong, Takashi Taniguchi, and Masahiro Ohshima. Nanoporous structure of the cell walls of polycarbonate foams. *Journal of materials science*, 49:2605–2617, 2014.

3. Felix M Büttner, Katharina Faulhaber, Karl Forchhammer, Iris Maldener, and Thilo Stehle. Enabling cell–cell communication via nanopore formation: structure, function and localization of the unique cell wall amidase amic2 of nostoc punctiforme. *The FEBS journal*, 283(7):1336–1350, 2016.

4. ANTONY Bacic, PHILIP J Harris, and BRUCE A Stone. Structure and function of plant cell walls. *The biochemistry of plants*, 14:297–371, 1988.

5. Kenneth Keegstra. Plant cell walls. *Plant physiology*, 154(2):483–486, 2010.

6. Neil AR Gow, Jean-Paul Latge, and Carol A Munro. The fungal cell wall: structure, biosynthesis, and function. *Microbiology spectrum*, 5(3):5–3, 2017.

7. Stephen J Free. Fungal cell wall organization and biosynthesis. *Advances in genetics*, 81:33–82, 2013.

8. Thomas J Silhavy, Daniel Kahne, and Suzanne Walker. The bacterial cell envelope. *Cold Spring Harbor perspectives in biology*, 2(5):a000414, 2010.

9. Waldemar Vollmer, Didier Blanot, and Miguel A De Pedro. Peptidoglycan structure and architecture. *FEMS microbiology reviews*, 32(2):149–167, 2008.

10. N. Carpita, D. Sabularse, D. Montezinos, and D. P. Delmer. Determination of the pore size of cell walls of living plant cells. *Science*, 205(4411):1144–7, 1979.

11. Andrew R Kirby, A Patrick Gunning, Keith W Waldron, Victor J Morris, and Annie Ng. Visualization of plant cell walls by atomic force microscopy. *Biophysical Journal*, 70(3):1138–1143, 1996.

12. Jgd Nobel and J. A. Barnett. Passage of molecules through yeast cell walls: A brief essay-review. *Yeast*, 7(4):313–323, 1991.

13. Rene Scherrer, Louise Louden, and Philipp Gerhardt. Porosity of the yeast cell wall and membrane. *Journal of bacteriology*, 118(2):534–540, 1974.

14. E. Atilgan, V. Magidson, A. Khodjakov, and F. Chang. Morphogenesis of the fission yeast cell through cell wall expansion. *Current biology: CB*, 25(16), 2015.

15. Tania Gualtieri, Enrico Ragni, Luca Mizzi, Umberto Fascio, and Laura Popolo. The cell wall sensor wsc1p is involved in reorganization of actin cytoskeleton in response to hypo-osmotic shock in saccharomyces cerevisiae. *Yeast*, 21(13):1107–1120, 2004.

16. Stefan Hohmann. Osmotic stress signaling and osmoadaptation in yeasts. *Microbiology and molecular biology reviews*, 66(2):300–372, 2002.

17. Stefan Hohmann, Marcus Krantz, and Bodil Nordlander. Yeast osmoregulation. *Methods in enzymology*, 428:29–45, 2007.

18. Jose Manuel Rodríguez-Peña, Raúl García, César Nombela, and Javier Arroyo. The high-osmolarity glycerol (hog) and cell wall integrity (cwi) signalling pathways interplay: a yeast dialogue between mapk routes. *Yeast*, 27(8):495–502, 2010.

19. Enrique R Rojas and Kerwyn Casey Huang. Regulation of microbial growth by turgor pressure. *Current Opinion in Microbiology*, 42:62–70, 2018.

20. Rui Ma and Julien Berro. Endocytosis against high turgor pressure is made easier by partial protein coating and a freely rotating base. *Biophysical Journal*, 120(3):52a, 2021.

21. Nicolas Minc, Arezki Boudaoud, and Fred Chang. Mechanical forces of fission yeast growth. *Current Biology*, 19(13):1096–1101, 2009.

22. Roshni Basu, Emilia Laura Munteanu, and Fred Chang. Role of turgor pressure in endocytosis in fission yeast. *Molecular biology of the cell*, 25(5):679–687, 2014.

23. Michal Skruzny, Thorsten Brach, Rodolfo Ciuffa, Sofia Rybina, Malte Wachsmuth, and Marko Kaksonen. Molecular basis for coupling the plasma membrane to the actin cytoskeleton during clathrin-mediated endocytosis. *Proceedings of the National Academy of Sciences*, 109(38):E2533–E2542, 2012.

24. Amir Sanati Nezhad, Mahsa Naghavi, Muthukumaran Packirisamy, Rama Bhat, and Anja Geitmann. Quantification of the young's modulus of the primary plant cell wall using bending-lab-on-chip (bloc). *Lab on a chip*, 13, 04 2013.

25. David Pereira, Thomas Alline, and Atef Asnacios. In vivo measurement of the young's modulus of the cell wall of single root hairs. *bioRxiv*, pages 2022–12, 2022.

26. John D Stenson, Peter Hartley, Changxiang Wang, and Colin R Thomas. Determining the mechanical properties of yeast cell walls. *Biotechnology progress*, 27(2):505–512, 2011.

27. AE Smith, KE Moxham, and APJ Middelberg. Wall material properties of yeast cells. part ii. analysis. *Chemical Engineering Science*, 55(11):2043–2053, 2000.

28. W Helfrich. Elastic properties of lipid bilayers: Theory and possible experiments:. *Zeitschrift für Naturforschung C*, 28(11-12):693–703, 1973.

29. Udo Seifert. Configurations of fluid membranes and vesicles. *Advances in physics*, 46(1):13–137, 1997.

30. Udo Seifert, Karin Berndl, and Reinhard Lipowsky. Shape transformations of vesicles: Phase diagram for spontaneous- curvature and bilayer-coupling models. *Phys. Rev. A*, 44:1182–1202, Jul 1991.

31. F Jülicher and U. Seifert. Shape equations for axisymmetric vesicles: A clarification. *Physical Review E*, 49(5):4728–4731, 1994.

32. Fanlong Meng, Jeff ZY Chen, Masao Doi, and Zhongcan Ouyang. Phase diagrams and interface in inflating balloon. *AIChE Journal*, 60(4):1393–1399, 2014.

33. Andrea Giudici and John S Biggins. Giant deformations and soft-inflation in lce balloons. *Europhysics Letters*, 132(3):36001, 2020.

34. Andrea Giudici and John S Biggins. Ballooning, bulging, and necking: An exact solution for longitudinal phase separation in elastic systems near a critical point. *Physical Review E*, 102(3):033007, 2020.

35. Ingo Müller and Peter Strehlow. *Rubber and rubber balloons: paradigms of thermodynamics*, volume 637. Springer Science & Business Media, 2004.

36. A Mallock. Ii. note on the instability of india-rubber tubes and balloons when distended by fluid pressure. *Proceedings of the Royal Society of London*, 49(296-301):458–463, 1891.

37. Andrew I Shevchuk, Pavel Novak, Marcus Taylor, Ivan A Diakonov, Azza Ziyadeh-Isleem, Marc Bitoun, Pascale Guicheney, Max J Lab, Julia Gorelik, Christien J Merrifield, et al. An alternative mechanism of clathrin-coated pit closure revealed by ion conductance microscopy. *Journal of Cell Biology*, 197(4):499–508, 2012.

38. Sari Tojkander, Gergana Gateva, and Pekka Lappalainen. Actin stress fibers–assembly, dynamics and biological roles. *Journal of cell science*, 125(8):1855–1864, 2012.

39. Yuko Sekino, Nobuhiko Kojima, and Tomoaki Shirao. Role of actin cytoskeleton in dendritic spine morphogenesis. *Neurochemistry international*, 51(2-4):92–104, 2007.

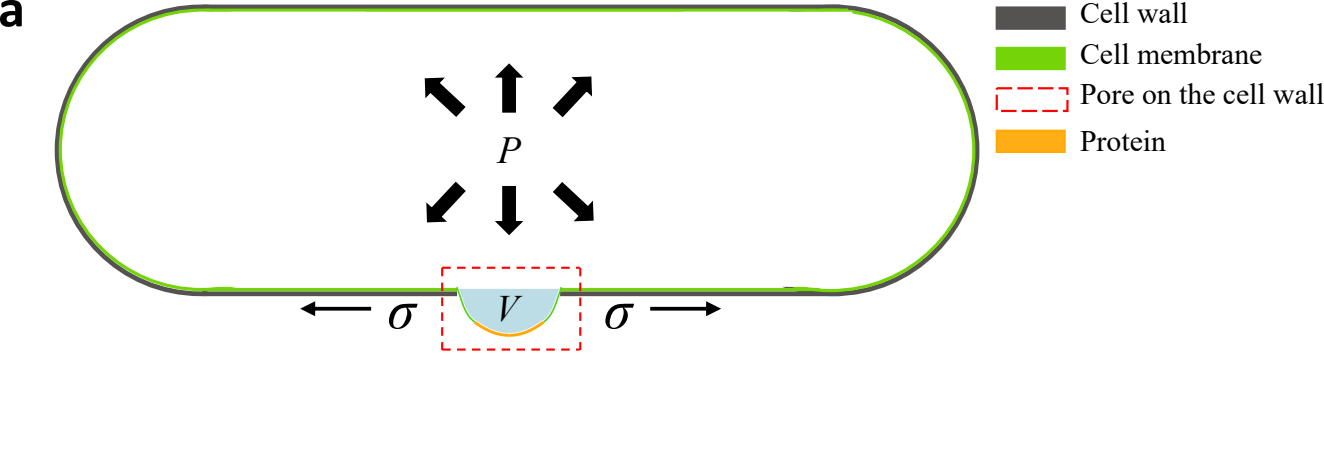
a
Cell wall
Cell membrane
Pore on the cell wall
Protein
P
V
σ
σ
b
Free-hinge
Fixed-hinge
Inside
p
r
z
u = 1
u = 0
ψ
Cell wall
Cell wall

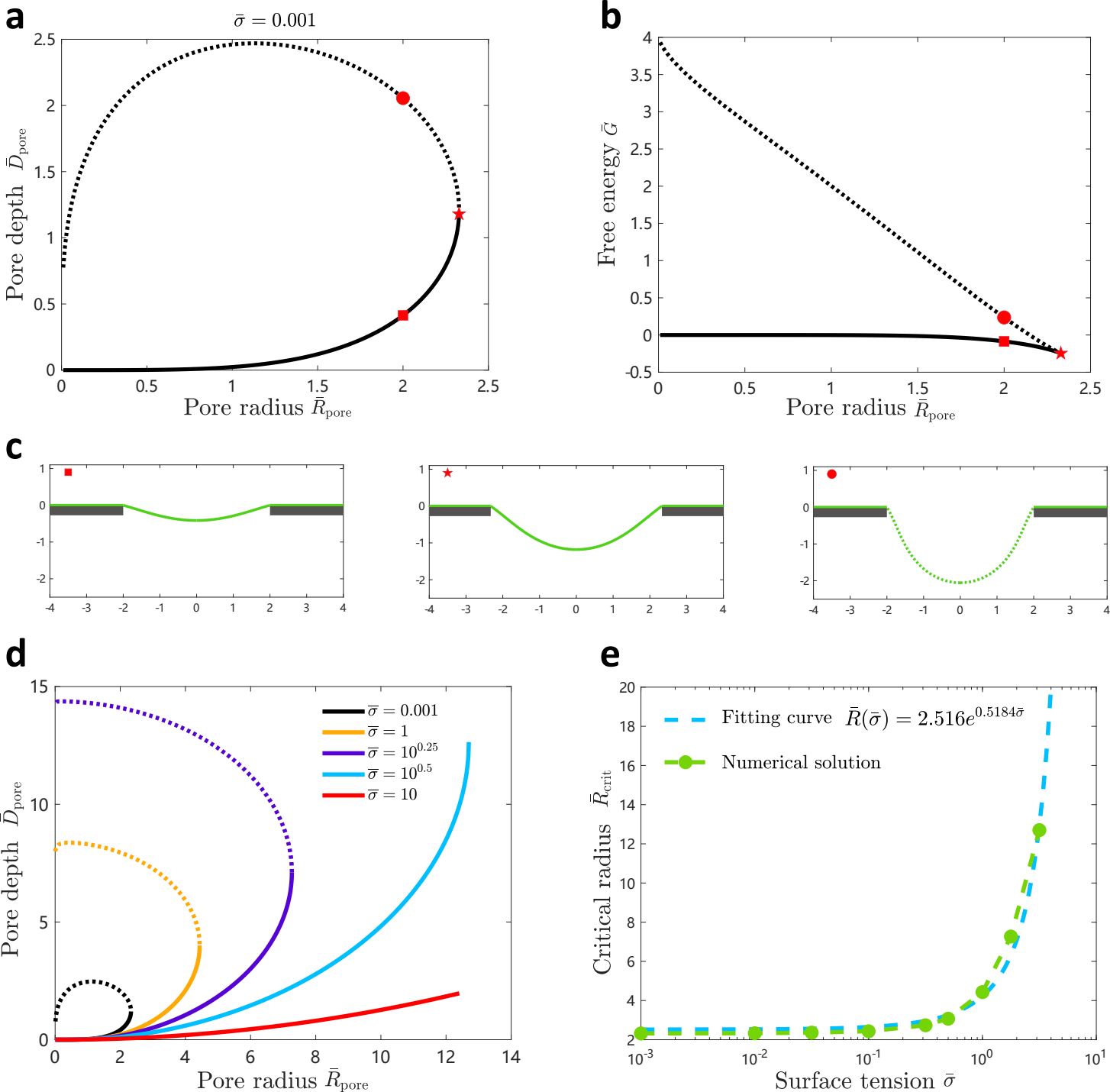
a
$\bar{\sigma} = 0.001$
Pore depth $\bar{D}_{\text{pore}}$
Pore radius $\bar{R}_{\text{pore}}$
b
Free energy $\bar{G}$
Pore radius $\bar{R}_{\text{pore}}$
c
d
$\bar{\sigma} = 0.001$
$\bar{\sigma} = 1$
$\bar{\sigma} = 10^{0.25}$
$\bar{\sigma} = 10^{0.5}$
$\bar{\sigma} = 10$
Pore depth $\bar{D}_{\text{pore}}$
Pore radius $\bar{R}_{\text{pore}}$
e
Fitting curve $\bar{R}(\bar{\sigma}) = 2.516e^{0.5184\bar{\sigma}}$
Numerical solution
Critical radius $\bar{R}_{\text{crit}}$
Surface tension $\bar{\sigma}$

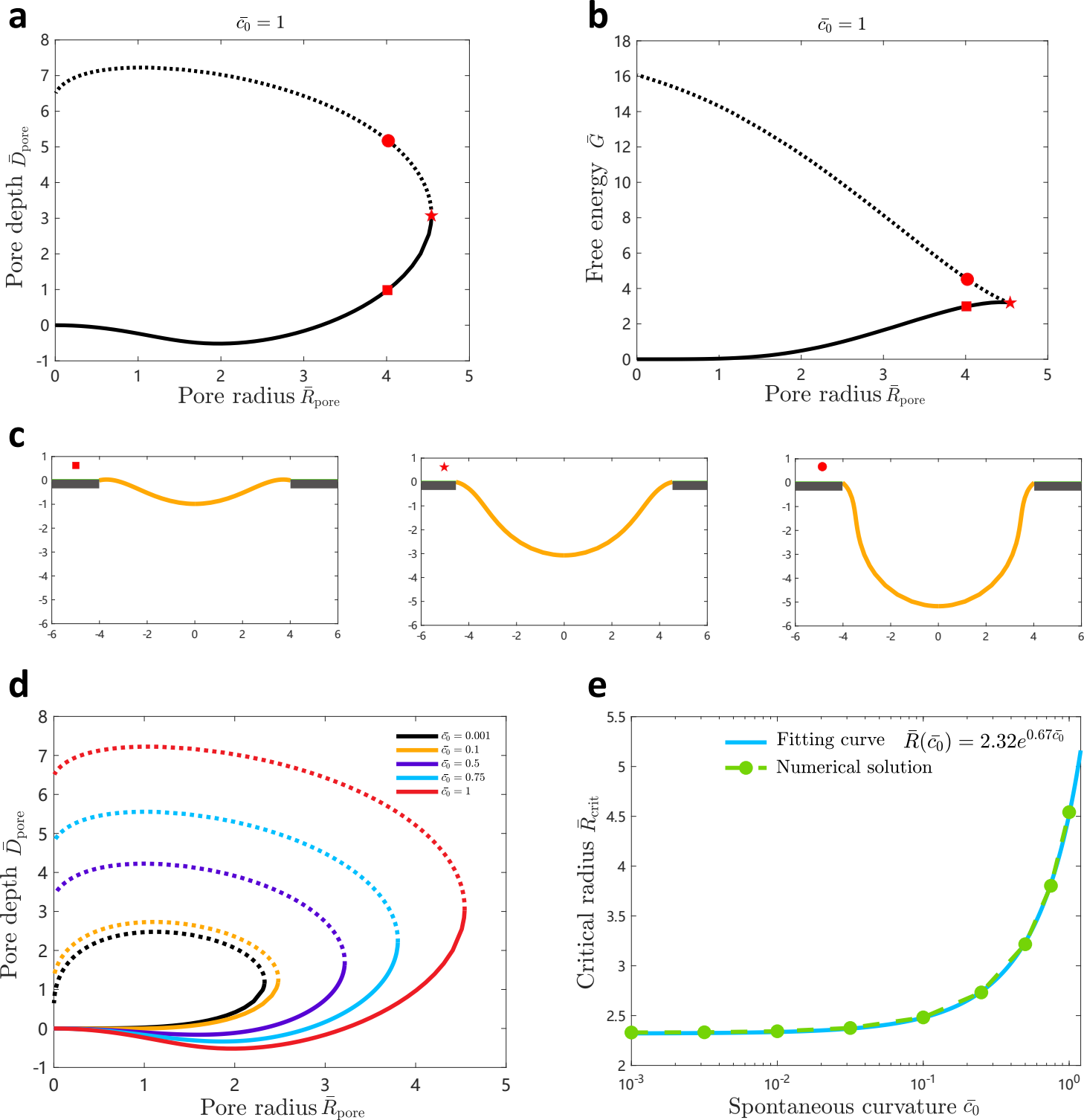
a
$\bar{c}_0 = 1$
Pore depth $\bar{D}_{\text{pore}}$
Pore radius $\bar{R}_{\text{pore}}$
b
$\bar{c}_0 = 1$
Free energy $\bar{G}$
Pore radius $\bar{R}_{\text{pore}}$
c
d
$\bar{c}_0 = 0.001$
$\bar{c}_0 = 0.1$
$\bar{c}_0 = 0.5$
$\bar{c}_0 = 0.75$
$\bar{c}_0 = 1$
Pore depth $\bar{D}_{\text{pore}}$
Pore radius $\bar{R}_{\text{pore}}$
e
Fitting curve $\bar{R}(\bar{c}_0) = 2.32e^{0.67\bar{c}_0}$
Numerical solution
Critical radius $\bar{R}_{\text{crit}}$
Spontaneous curvature $\bar{c}_0$

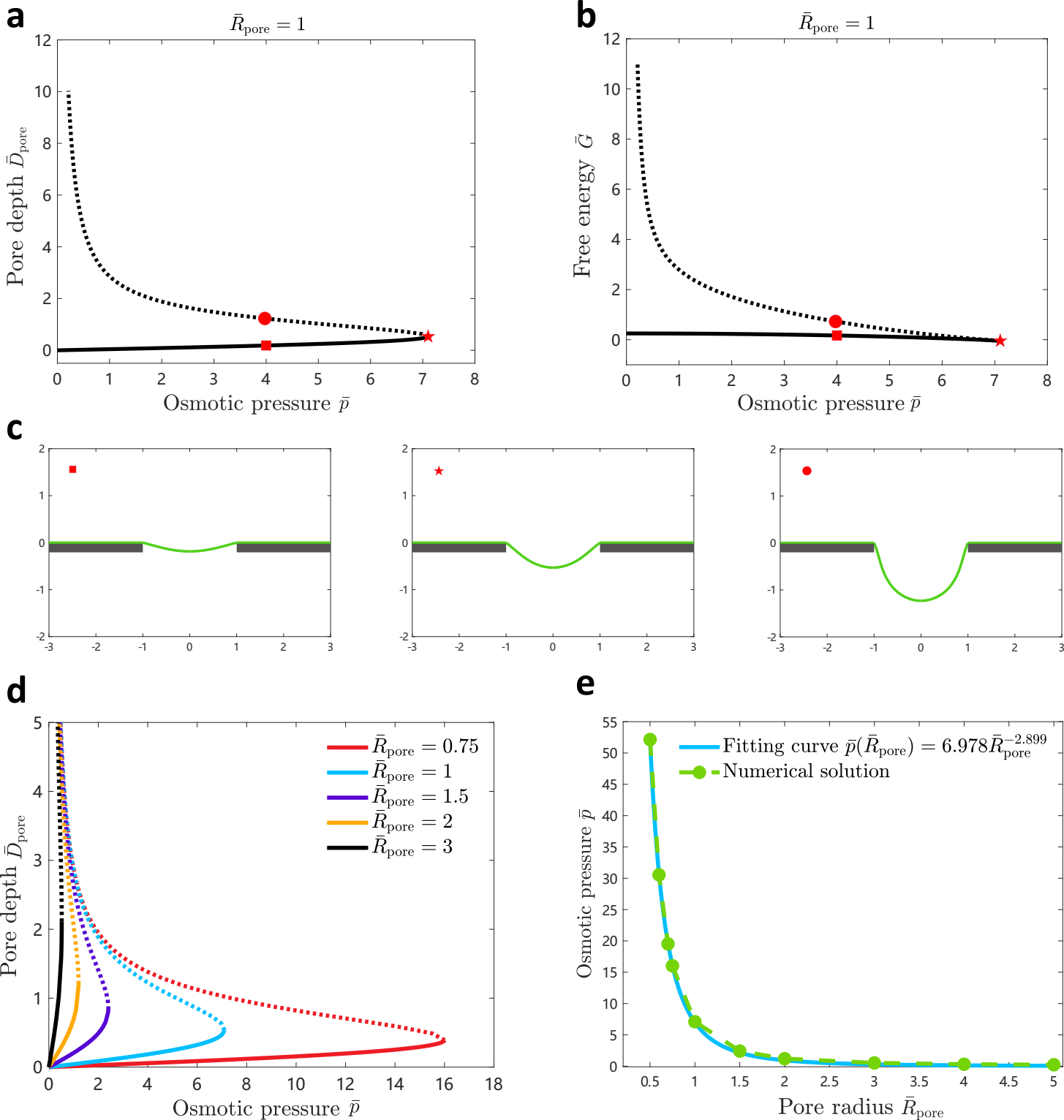
a
$\bar{R}_{\text{pore}} = 1$
Pore depth $\bar{D}_{\text{pore}}$
Osmotic pressure $\bar{p}$
b
$\bar{R}_{\text{pore}} = 1$
Free energy $\bar{G}$
Osmotic pressure $\bar{p}$
c
d
$\bar{R}_{\text{pore}} = 0.75$
$\bar{R}_{\text{pore}} = 1$
$\bar{R}_{\text{pore}} = 1.5$
$\bar{R}_{\text{pore}} = 2$
$\bar{R}_{\text{pore}} = 3$
Pore depth $\bar{D}_{\text{pore}}$
Osmotic pressure $\bar{p}$
e
Fitting curve $\bar{p}(\bar{R}_{\text{pore}}) = 6.978\bar{R}_{\text{pore}}^{-2.899}$
Numerical solution
Osmotic pressure $\bar{p}$
Pore radius $\bar{R}_{\text{pore}}$

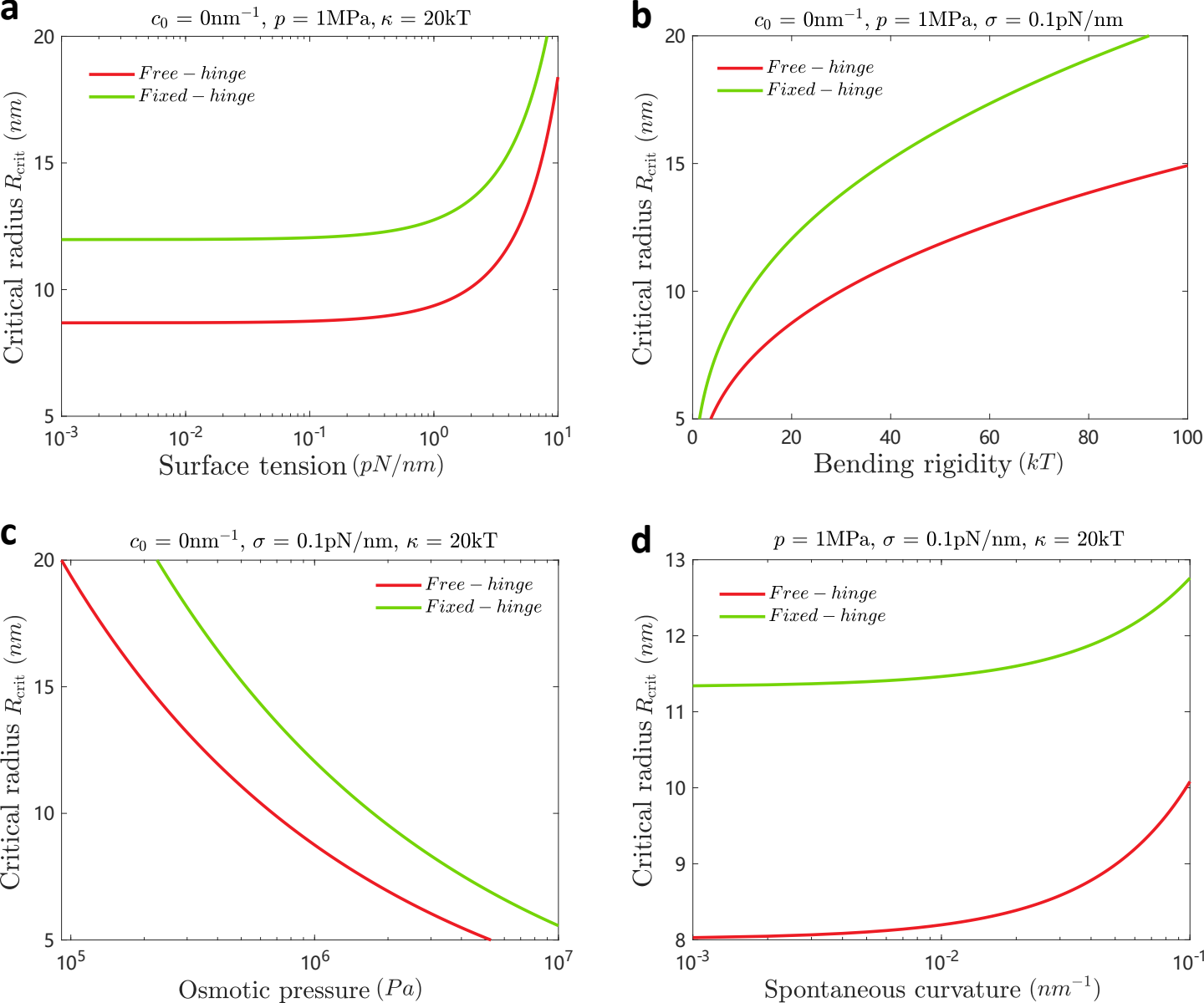
a
$c_0 = 0\text{nm}^{-1}$, $p = 1\text{MPa}$, $\kappa = 20\text{kT}$
Free − hinge
Fixed − hinge
Critical radius R_{crit} (nm)
Surface tension (pN/nm)
b
$c_0 = 0\text{nm}^{-1}$, $p = 1\text{MPa}$, $\sigma = 0.1\text{pN/nm}$
Free − hinge
Fixed − hinge
Critical radius R_{crit} (nm)
Bending rigidity (kT)
c
$c_0 = 0\text{nm}^{-1}$, $\sigma = 0.1\text{pN/nm}$, $\kappa = 20\text{kT}$
Free − hinge
Fixed − hinge
Critical radius R_{crit} (nm)
Osmotic pressure (Pa)
d
$p = 1\text{MPa}$, $\sigma = 0.1\text{pN/nm}$, $\kappa = 20\text{kT}$
Free − hinge
Fixed − hinge
Critical radius R_{crit} (nm)
Spontaneous curvature (nm^{-1})